1 **Unraveling the role of polysaccharide-goethite associations on**

2 **glyphosate' adsorption-desorption dynamics and binding**

3 **mechanisms**

4

5

6

7 *Behrooz Azimzadeh and Carmen Enid Martínez**

8 Soil and Crop Sciences, School of Integrative Plant Science, College of Agriculture and Life

9 Sciences, Cornell University, Ithaca, New York 14853, USA

10

11

12

13

14

15

16 **Corresponding author**: Carmen Enid Martínez, Soil and Crop Sciences, School of Integrative

17 Plant Science, College of Agriculture and Life Sciences, Cornell University, Ithaca, New York

18 14853, USA Tel: +1 (607) 255-0895, E-mail: cem20@cornell.edu

19

20

21

26

27

28 **Abstract**

29 *Hypothesis*

30 Glyphosate retention at environmental interfaces is strongly governed by adsorption and

31 desorption processes. In particular, glyphosate can react with organo-mineral associations

32 (OMAs) in soils, sediments, and aquatic environments. We hypothesize mineral-adsorbed

33 biomacromolecules modulate the extent and rate of glyphosate adsorption and desorption where

34 electrostatic and noncovalent interactions with organo-mineral surfaces are favored.

35 *Experiments*

36 Here we use *in-situ* attenuated total reflectance Fourier-transform infrared, X-ray photoelectron

37 spectroscopy, and batch experiments to characterize glyphosate's adsorption and desorption

38 mechanisms and kinetics at an organo-mineral interface. Model polysaccharide-goethite OMAs

39 are prepared with a range of organic (polysaccharide, PS) surface loadings. Sequential

40 adsorption-desorption studies are conducted by introducing glyphosate and background

41 electrolyte solutions, respectively, to PS-goethite OMAs.

42 *Findings*

43 We find the extent of glyphosate adsorption at PS-goethite interfaces was reduced compared to

44 that at the goethite interface. However, increased polysaccharide surface loading resulted in

45 lower relative glyphosate desorption. At the same time, increase PS surface loading yielded

46 slower glyphosate adsorption and desorption kinetics compared to corresponding processes at the

47 goethite interface. We highlight that adsorbed PS promotes the formation of weak noncovalent

48 interactions between glyphosate and PS-goethite OMAs, including the evolution of hydrogen

49 bonds between (*i*) the amino group of glyphosate and PS and (*ii*) the phosphonate group of

2

50   glyphosate and goethite. It is also observed that glyphosate's phosphonate group preferentially

51   forms inner-sphere monodentate complexes with goethite in PS-goethite whereas bidentate

52   configurations are favored on goethite.

53

54   **1. Introduction**

55   Glyphosate (*N*-(phosphonomethyl)glycine) is applied to agricultural crops, side roads, and

56   individuals' home gardens and lawns. Upon application, glyphosate interacts with mineral and

57   organic-coated mineral surfaces potentially affecting its mobility and efficacy as an herbicide.

58   Since the mobility and distribution of herbicides in soil is generally mediated by water transport,

59   adsorption-desorption processes at these interfaces are deemed important. Glyphosate is the

60   world's most heavily applied herbicide [1] and its widespread use has raised concerns about its

61   effects on human health and the environment [2-4].

62   Glyphosate is a polar organic molecule and a zwitterion at relevant environmental conditions,

63   with a tridentate character due to its amino, carboxylic, and phosphonic functional groups [5, 6].

64   A large number of studies show that glyphosate can strongly interact with metal ions in solution

65   and at water-mineral interfaces [4, 5, 7-10], particularly with iron (hydr)oxides through its

66   phosphonic group [7-9, 11-15]. The role of organic-coated mineral surfaces (i.e., organo-mineral

67   associations, OMAs) on the retention, mobility and distribution of glyphosate in soils is far less

68   studied and understood. A few studies have shown that OMAs may inhibit, hinder or enhance the

69   mobility of glyphosate in the environment [12, 16]. For example, humic acid-goethite

70   associations have been shown to increase glyphosate mobility, presumably a result of

71   electrostatic repulsion due to the negative charge conferred by sorbed humic acid and by a

72   reduction in the availability of active mineral surface sites [12]. Conversely, a more recent study

73   [16] demonstrated that a humic acid-kaolinite association can adsorb higher amounts of

74   glyphosate than kaolinite alone. In the latter study, the authors suggest a ternary adsorption

75   system in which glyphosate binds to the interfacial hydroxyl groups in humic acid-kaolinite

76   associations via hydrogen bonds involving carboxyl, amino, and phosphonyl functional groups

77   of glyphosate. Based on these disparate results, we are unable to conceptualize or predict the

78   effect OMAs might have on glyphosate retention. Besides, previous studies have failed to

79   consider desorption dynamics when assessing glyphosate behavior at these heterogeneous

80   organo-mineral interfaces and have used humic acids as model organic coatings. Humic acids

81   (together with fulvic acids) are an operationally defined organic fraction extracted from soils and

82   do not represent the biomolecules present in soils [17].

83   To address this void in knowledge, we present a series of molecular-scale, time-resolved, and

84   surface-sensitive adsorption-desorption studies using goethite and polysaccharide-goethite

85   associations as model interfaces. A clear understanding of the molecular structure of an OMA is

86   essential to accurately probe glyphosate behavior and fate. We used goethite (α-FeOOH) as the

87   model mineral in experiments because it is commonly present in soils and frequently used in

88   glyphosate sorption studies [9, 12, 14, 18-21]. We chose a polysaccharide (i.e., a naturally

89   occurring biomacromolecule present in plant cell walls and therefore a major component of

90   organic matter in soils) as the model organic molecule present in OMAs. Polysaccharides (PS)

91   are ubiquitous in soils and potentially act as binding agents in the soil matrix [22, 23]. Unlike

92   humic and fulvic acids, the structure of the chosen PS (pectin) is well-known: a linear polymer

93   composed of α-1,4-linked galacturonic acid units. The galacturonic acid units could be

94   methoxylated and/or amidated to various degrees [24, 25].

95   In this study, we determine the extent, kinetics and mechanisms of interaction of glyphosate at

96   PS-goethite and goethite interfaces and investigate the effect increasing polysaccharide surface

97   loading might have on these processes. All experiments were conducted at pH = 5.0 to simulate

98   agricultural soils of humid climates where the affinity of glyphosate for soil particles is high and

99   where soils are rich in iron (hydr)oxides and organic matter [26-28]. Experimentally, we use *in-*

100   *situ* time-resolved attenuated total reflectance Fourier transform infrared (ATR-FTIR)

101   spectroscopy to obtain adsorption-desorption kinetic parameters and to decipher glyphosate's

102   mechanisms of interaction. The capabilities of ATR-FTIR to obtain kinetic information of

103   environmentally relevant systems has been demonstrated in several studies [12, 29, 30]. Batch

104   and X-ray photoelectron spectroscopy (XPS) experiments are conducted to further characterize

105   the extent of glyphosate adsorption-desorption dynamics at PS-goethite interfaces. The use of

106   XPS to acquire surface coverage and chemical bonding information at glyphosate-mineral and

107   biomolecule-mineral interfaces has been established [9, 31, 32]. In addition, a homonuclear

108   proton saturation transfer difference nuclear magnetic resonance (STD-NMR) experiment [33]

109   was conducted to learn whether glyphosate and PS molecules interact in solution.

110   Furthermore, we decipher the contribution of each functional group of glyphosate (amino,

111   carboxylate, phosphonate) to its interaction with goethite and with polysaccharide-goethite

112   associations during adsorption and desorption processes. To the best of our knowledge, this is the

113   first study highlighting glyphosate's adsorption-desorption dynamics at polysaccharide-goethite

114   interfaces at the molecular-scale, in solution and in real time. These studies provide new

115   knowledge that further our understanding of glyphosate's sorption-desorption dynamics at

116   heterogeneous organo-mineral interfaces.

117

118   ## 2. Materials and Methods

119   ### 2.1. Materials

120   Glyphosate (96 % purity) was purchased from Sigma-Aldrich (Milwaukee, USA). Amidated

121   high methoxyl pectin was acquired from Sigma-Aldrich. This pectin, a polysaccharide (PS), is

122   used as the model biomacromolecule in our study and it has a MW of $\approx$ 71100 g mol^{-1} [34-36],

123   and a p$K_{a(COOH)}$ = 3.3 – 4.5 [37]. The galacturonic acid (GalA), methoxy and amide contents

124   were calculated as 37.1, 58.7, 4.2 %, respectively (see SM1 in supplementary information (SI)

125   for details). All solutions and suspensions were made with deionized water (18.2 MΩ resistance),

126   boiled and purged with N_2 gas to remove dissolved CO_2. In all experiments, a 10 mM KCl

127   background electrolyte was used to approximate the low ionic strength of soil solutions. Goethite

128   (α-FeOOH) was synthesized by the method of Schwertmann and Cornell [38]. Details of mineral

129   synthesis and characterization can be found in SI (SM2 and Figure S1). The pH at the point of

130   zero charge (pH$_{pzc}$) of the synthesized goethite was 8.4 $\pm$ 0.2 (Figure S2 in SI).

131

132   ### 2.2. ^{1}H Saturation-transfer difference (STD) NMR experiment

133   Saturation transfer difference (STD) NMR experiments were used to probe potential

134   interactions between glyphosate and the PS in solution. For the most sensitive STD-NMR

135   spectra, a 20 μM PS solution was prepared in D_2O (99.9 atom % D, Cambridge Isotope

136   Laboratories Inc.). Then, 0.35 mg glyphosate was dissolved in 2 mL of the PS solution

137   ([glyphosate] = 1.0 mM) to yield a 50-fold excess glyphosate to ligand (PS) ratio [39]. The pH

138   was adjusted to 5 using potassium deuteroxide (40 wt % in D_2O, $\geq$ 99 atom % D, Sigma) and

139   deuterium chloride (35 wt % in D_2O, $\geq$ 99 atom % D, Sigma). ^{1}H STD-NMR experiments were

140   conducted on a 600 MHz Varian Inova NMR spectrometer at 25 °C. STD parameters were

141   selected based on values reported in a previous study [33]. Spectra were processed in MNova

142   software (v. 14.3, Mestrelab Research S.L.).

143

144   **2.3. Batch experiments, XPS and zeta potential analyses**

145   Batch adsorption-desorption studies were conducted to quantify glyphosate adsorption and

146   desorption from experimental surfaces, and to obtain qualitative and quantitative information

147   about the surface characteristics and bonding environment of complexes using zeta potential and

148   X-ray photoelectron spectroscopy (XPS) measurements. Procedural details of the batch

149   experiments are described in SI, SM3). Briefly, a series of PS-goethite OMAs were synthesized

150   with varying PS surface loading (i.e., Phases 1 and 2). Then, glyphosate adsorption and

151   desorption experiments were conducted at pH 5 by addition of a 1 mM glyphosate solution to the

152   prepared PS-goethite OMAs (adsorption, Phase 3), followed by desorption (Phase 4) using a 10

153   mM KCl background solution. The supernatants were filtered (0.2 μm) and analyzed using a

154   TOC-L analyzer (Shimadzu Scientific Instruments) along with standard polysaccharide

155   solutions. Glyphosate concentrations were also measured using a colorimetric approach after

156   derivatization in 2 mM fluorenyl orthochloroformate and 20 mM borate buffer solutions [40, 41].

157   XPS analyses were conducted on selected pellets and required standards. Details of XPS

158   analyses are presented in SI, SM4. For zeta potential measurements, all of the pellets were

159   resuspended in background solution and measured with a Zetasizer (Nano ZS90, Malvern

160   instruments Ltd., UK). BET surface area (N_2 adsorption) and scanning electron microscopy

161   (SEM) images were obtained with an ASAP2460 instrument (Micromeritics Instrument Corp.)

162   and a Zeiss Gemini 500 FE-SEM, respectively.

163

164 **2.4. *In-situ* time-resolved ATR-FTIR Adsorption-desorption Experiments**

165   The workflow of *in-situ* ATR-FTIR (attenuated total reflectance Fourier transform infrared)

166 experiments (Figure S3) and methodological details are reported in SI (SM5 and SM6). The

167 formation of PS-goethite complexes was initiated by introducing PS solutions over a hydrated

168 layer of goethite on the surface of the ATR crystal. A range of surface loadings were obtained by

169 passing different initial concentrations of PS ([PS] = 0, 4, 8, 14, 28, 42, and 56 μM) over goethite

170 films for a fixed time (coating, Phase 1 ≈ 180 min). Adsorbed PS was stabilized by passing 10

171 mM KCl background electrolyte to remove any loosely bound PS. Stability of PS-goethite

172 complexes was considered attained when no changes were observed in interfacial spectra

173 collected during background solution flow (stabilization, Phase 2 ≈ 60 min). At this point, a

174 background spectrum was collected, and adsorption of glyphosate was initiated by exchanging

175 the background solution with a fixed 4.0 mM glyphosate solution (adsorption, Phase 3 ≈ 86 min).

176 Glyphosate adsorption was followed by a desorption experiment using the same background

177 solution until equilibrium (desorption, Phase 4 ≈ 72 min). Solutions with a pH of 5.0 were used

178 for all experiments, which model environmentally relevant conditions representative of

179 agricultural soils of humid regions (I =10 mM and pH = 5.0). The pH was maintained within

180 0.05 pH units by regulated additions of 0.005 M HCl or KOH with a pH controller. Experiments

181 were repeated 4 times on freshly prepared films under identical conditions. All the *in-situ*

182 experiments were conducted under ambient atmosphere and using a close flow through system at

183 a rate of 0.85 ± 0.05 mL min^{-1} (flow velocity = 4.5×10^{-3} m s^{-1}) using a peristaltic pump (Cole-

184 Parmer, IL). Bulk solution spectra of glyphosate and polysaccharide were collected at

185 concentrations of 0.10 M and 8.0 mg mL^{-1}, respectively, in a 10 mM KCl background solution at

186 pH = 5.0. All spectra were collected by subtracting the spectrum of the background electrolyte

187   from the spectrum of each sample. In this way, the difference spectrum contains only the

188   absorption bands of interfacial species, including inner- and outer- sphere species and bands of

189   free or uncomplexed species in the bulk solutions.

190

191   **2.5. ATR-FTIR Data Processing for Analyses**

192   Two regions, the phosphonate frequency region ($1100 - 950$ cm^{-1}, $v(PO)$) and the carboxylate-

193   amine frequency region ($1700 - 1500$ cm^{-1}, $v(CAc)$), were cut and further processed. The integral

194   of the baseline-corrected IR peaks of the phosphonate region was used to probe total glyphosate

195   adsorption and desorption kinetics and P-O band coordination to Fe(III). The spectral features in

196   the 1700-1500 cm^{-1} range were deconvoluted in order to determine potential hydrogen bonding

197   and the contribution of carboxylate ($v_{as}(COO^-)$) and amine ($\delta(NH_2^+)$) functionalities in interfacial

198   complex formation and subsequent dynamicity of adsorbed glyphosate. Deconvolution of the

199    $v(CAc)$ band at the goethite and PS-goethite interfaces is fully explained in SI, SM7. Peak fitting

200   of the spectra was carried out using a second derivative deconvolution algorithm using PeakFit

201   package v.4.12 (Systat Software Inc., San Jose, CA).

202

203   **2.6. Glyphosate Adsorption-desorption Kinetic Models**

204   Integral of FTIR bands ($A(\tilde{v}_i)$) of glyphosate moieties during adsorption and desorption

205   experiments were fitted with two commonly used kinetic models, the Lagergren's pseudo-

206   second-order (PSO) and pseudo-first-order (PFO) models, respectively [42, 43]. The PSO model

207   for adsorption processes can be described by the following equation [44]:

$$A(\tilde{v}_i)_{t,ads} = \frac{k_{2,ads} A(\tilde{v}_i)^2_{e,ads} t}{1 + k_{2,ads} A(\tilde{v}_i)_{e,ads} t} \qquad \text{(Eq. 1)}$$

208   where $A(\tilde{v}_i)_{t,ads}$ is the integral absorption intensity of the glyphosate band (a.u.) at adsorption time

209   t (min), $k_{2,ads}$ is the PSO rate constant (min^{-1} a.u.$^{-1}$), and $A(\tilde{v}_i)_{e,ads}$ is the integral absorption

210   intensity of the glyphosate band at equilibrium (a.u.).

211   Desorption of glyphosate was described by a modified PFO model represented by the

212   following equation [30]:

$$A(\tilde{v}_i)_{t,des} = (\alpha - A(\tilde{v}_i)_{e,des})e^{-k_{1,des}t} + \alpha \qquad \text{(Eq. 2)}$$

213   where $A(\tilde{v}_i)_{t,des}$ is the integral absorption intensity of the glyphosate band (a.u.) at desorption time

214   t (min), $k_{1,des}$ is the PFO rate constant (min^{-1}), $A(\tilde{v}_i)_{e,des}$ is the integral absorption intensity of the

215   glyphosate band at the end of the desorption phase (a.u.), and α is a dimensionless constant that

216   locates the desorption curve that follows just after the adsorption curve at equilibrium. The PFO

217   model was also applied to describe PS's adsorption and desorption kinetics at the goethite

218   interface during formation and stabilization of PS-goethite OMAs (see SI, SM8 for details). All

219   fitting was completed with the nonlinear curve fitting GraphPad Prism v.9.0 software (GraphPad

220   Inc, San Diego, CA).

221

222   **3. Results and Discussion**

223   **3.1 Glyphosate attaches to polysaccharide chains.**

224   The ^{1}H STD-NMR spectra of glyphosate with and without PS are shown in Figure 1. The

225   singlet peak (H1) corresponds to protons next to the glyphosate carboxyl group, while the

226   doublet (H2) derives from proton splitting due to geminal coupling with the P nucleus [33, 45].

227   Weak STD correlations were observed for the PS sample, indicating reversible association in

228   bulk solution. In fact, both H1 and H2 protons were visible in STD difference spectra indicating

229   glyphosate attach to hydrophilic moieties of PS chains through noncovalent interactions (Figure

230   1-a). As previously suggested, this result provides evidence of a host-guest complex formation

231   between glyphosate and PS, similar to that observed with other natural macromolecules [33, 46].
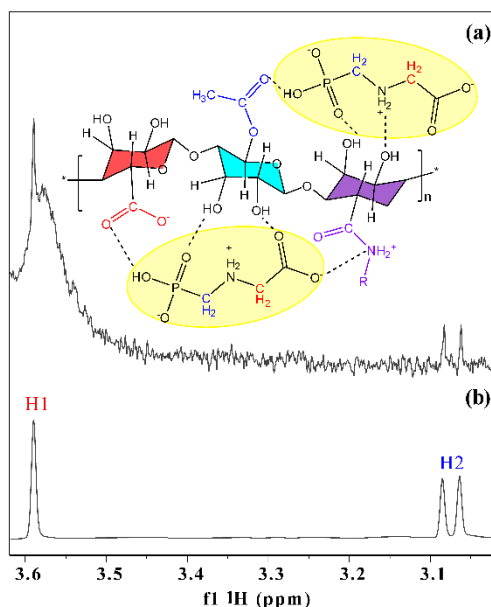
232

233   **Figure 1**. ^{1}H STD-NMR spectra at pH 5. (a) STD difference spectrum of a sample containing 0.1

234   mM glyphosate and 20 μM polysaccharide, together with a proposed structure for the PS-

235   glyphosate complex, and (b) reference ^{1}H spectrum of 1 mM glyphosate. Black dashed lines in

236   (a) represent noncovalent bonds. The full-range ^{1}H STD-NMR spectrum of the PS-glyphosate

237   complex is shown in Figure S4.

238

239   **3.2. Polysaccharide and goethite form organo-mineral associations.**

240   Interfacial ATR-FTIR spectra (Figure 2 A-1) indicate the progression of PS adsorption through

241   increasing signals of skeletal bands of the pyranose rings (e.g., $v(CC)(CO)_{ring}$) and α-1,4

242   glycosidic bonds (e.g., $v_{as}(COC)_g$) from $1200 - 950$ cm^{-1} [47-49]. Intense peaks within the 1780

243    $- 1200$ cm^{-1} range are also observed and are assigned to diverse band types, including

244   methylester (e.g., $v(C=O)_e$), amide (e.g., amide I and II) and carboxylate (e.g., $v_{as}(COO^-)$) of

245   residual groups in GalA rings [25, 37, 49-54]. A complete list of peak assignments is shown in

246   SI, Table S1. Kinetic data (Figure 2B), monitored using the $v(CO)(CC)_{ring}$ peak height, indicates

247   stable OMAs formed between PS and goethite with only a small fraction of adsorbed PS

248   removed from the surface at the end of the stabilization phase ($4.8 - 9.6\%$). The kinetics of PS

249   coating and stabilization are well described by a PFO model (Figure 2B, and Table S2).

250   Furthermore, estimated $k_{1,ads}$ and $k_{1,des}$ values indicate PS-goethite formation and stabilization are

251   faster with increasing PS concentration. As shown by identical surface morphology (texture) of

252   SEM images (imaging resolution of ≈ 5 nm), the PS seems to form evenly distributed coatings

253   on synthesized PS-goethite OMAs that result in significant reduction of BET surface area

254   (Figure 2C – D).

255
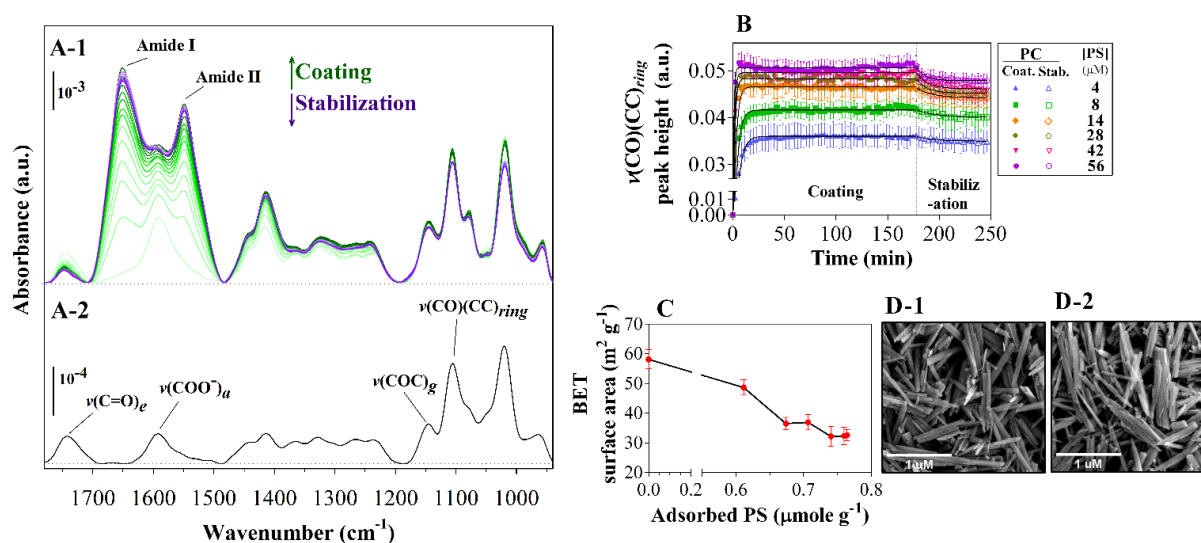
256   **Figure 2.** Formation and stability of PS-goethite OMAs. (A-1) Representative set of *in-situ*

257   ATR-FTIR spectra collected during PS's coating (green lines) and stabilization (purple lines)

258   over a goethite film ([PS] = 28 µM). Spectra collected every ≈ 8 minutes. (A-2) The solution

259   state spectrum for polysaccharide (112 µM in 10 mM KCl at pH 5.0). (B) Evolution of

260    $v(CO)(CC)_{ring}$ (1106 cm^{-1}) vibrations during coating and stabilization. (C) BET surface area of

261   PS-goethite OMAs as a function of adsorbed PS. (D) SEM image of (D-1) goethite and (D-2) a

262   PS-goethite OMA (PS ≈ 0.8 µmole g^{-1}).

263

264   **3.3. Glyphosate retention by PS-goethite organo-mineral associations**

265   Batch studies indicate glyphosate adsorption is diminished (52 – 37 %, Table S3) by adsorbed

266   PS (Figure 3A). The amount of glyphosate retained after desorption is also lower in PS-goethite

267   OMAs compared to goethite (% 30 – 13 decrease). However, a reversal to this trend is observed

268   at the highest PS loadings. Zeta potential measurements (Figure 3B) indicate PS-goethite and

269   glyphosate-PS-goethite complexes developed a negative surface charge whereas goethite (≈ 30

270   mV) and glyphosate-goethite (≈ 3 mV) are positively charged. Results also indicate the zeta

271   potential of PS-goethite and glyphosate-PS-goethite complexes decreases with increasing PS

272   loading. Decreased adsorption of glyphosate by PS-goethite OMAs relative to goethite can then

273   be explained by electrostatic repulsion between two negatively charged entities. Furthermore,

274   increases in PS surface loading, and corresponding decreases in SA (Figure 2C), limits the

275   surface available for adsorption of glyphosate on PS-goethite OMAs. Still, the trend reversal in

276   adsorbed and retained glyphosate corresponds to the extent of PS association on goethite (Figure

277   3A). As previously shown in STD difference spectra (Figure 1-a), the weak attachment of

278   glyphosate to PS may facilitate the retention of glyphosate molecules within adsorbed PS that

279   subsequently leads to this trend reversal. The mechanisms involved in these interactions are

280   discussed in the following sections.

281
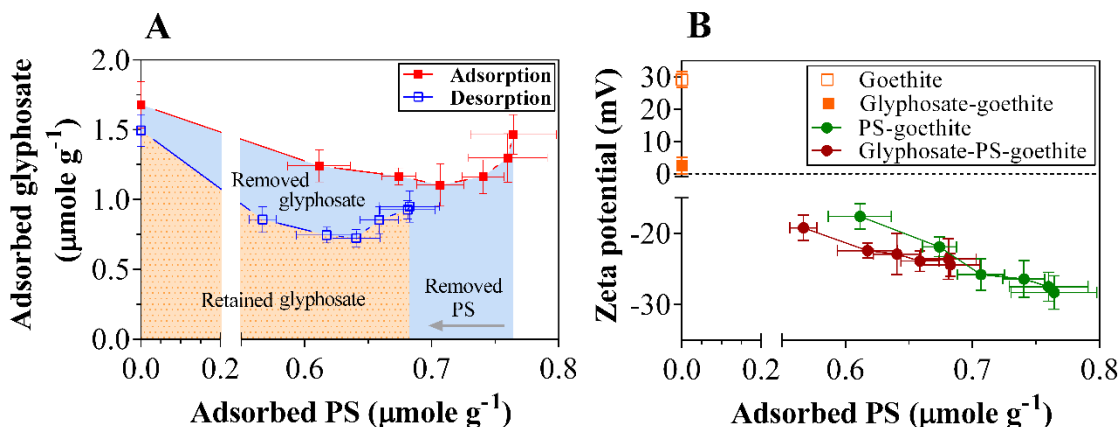
Figure 3. Results of batch experiments. Influence of adsorbed PS on (A) glyphosate's adsorption

and desorption dynamics and (B) zeta potential measurements. Blue and orange areas in A

represent the amount of glyphosate removed and retained at equilibrium, respectively. Error bars

represent standard deviation values from replicates (n = 3).

286

3.4. Contribution of glyphosate's functional groups to interfacial adsorption-desorption and kinetics.

Representative *in-situ* time-resolved ATR-FTIR spectra of glyphosate's retention dynamics at

the PS-goethite and goethite interface highlight the progression of glyphosate adsorption and

desorption through increases and decreases in intensity of the phosphonate, carboxylate, and

amine bands of the spectra (Figure 4A-1 and A-2). In our study, phosphonate ($v(PO)$, $1050 - 950$

cm^{-1}) and carboxylate-amine ($v(CAc)$, $1700 - 1500$ cm^{-1}) integrated band areas are considered a

measure of glyphosate's surface-associated species [8, 12]. Vibrational modes within the $v(PO)$

band area include inner-sphere (*IS*) (e.g., P-O-Fe) and outer-sphere (*OS*) (e.g., $(PO_3)_{OS}$ or

14

296    $(PO_2)_{OS}$) species [8, 9, 12, 14]. The carboxylate-amine $v(CAc)$ integrated band area includes

297   surface-associated $v_{as}(COO^-)$ and $\delta(NH_2^+)$ vibrational modes [7, 8, 21].

298   Increased PS loading in PS-goethite OMAs impacts glyphosate's adsorption-desorption

299   kinetics and the contribution of observed surface-associated bands (Figure 4). Consistent with

300   batch experiments, interfacial ATR results show a decrease in intensity of $v(PO)$ and $v(CAc)$

301   bands upon glyphosate interaction with PS-goethite OMAs compared to goethite (Figures 4B –

302   D). These results are in good agreement with Arroyave *et al* [12] where glyphosate adsorption

303   onto humic acid-goethite OMA was hindered, but it is contrary to the results of Guo *et al.* [16]

304   where higher amounts of glyphosate were adsorbed onto humic acid-kaolinite OMA. Variability

305   in the results might be explained by the stability of the OMAs, where humic acid and PS bind

306   strongly onto goethite whereas weak interactions dominate in humic acid-kaolinite OMA.
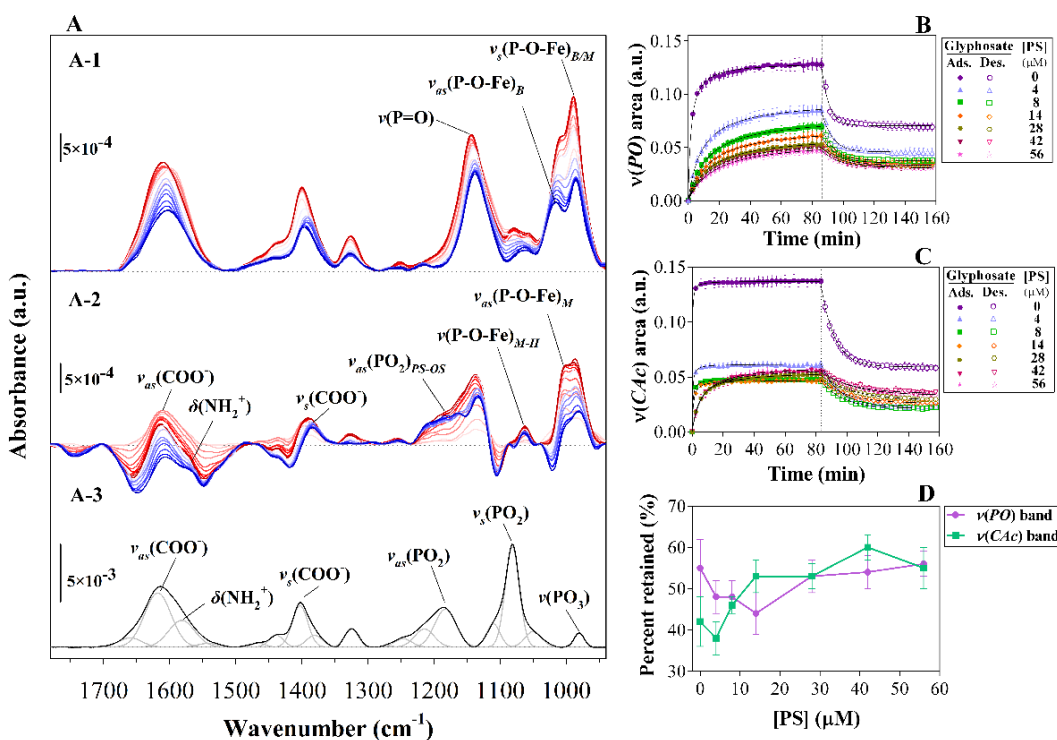
307

308 **Figure 4.** Representative time-resolved *in-situ* ATR-FTIR spectra collected during glyphosate

309 adsorption and desorption experiments at pH 5 on (A-1) goethite and (A-2) PS-goethite OMAs

310 ([PS] = 14 μM). Red and blue lines indicate the evolution of interfacial spectra collected every ≈

311 8 minutes. (A-3) Solution state ATR-FTIR spectrum of 0.1 M glyphosate in 10 mM KCl at pH

312 5.0; gray lines show deconvoluted IR components. Evolution of integrated (B) phosphonate

313 ($v(PO)$) and (C) carboxylate-amine ($v(CAc)$) bands of glyphosate with increased PS surface

314 loading. (D) shows the percentage of $v(CAc)$ and $v(PO)$ bands retained at the end of the

315 desorption phase (percentage retained = $[A(\tilde{v}_i)_{e,des}/A(\tilde{v}_i)_{e,ads}] \times 100]$).

316

317   Adsorption-desorption kinetics for $v(PO)$ and $v(CAc)$ bands were described by the PSO and

318 PFO kinetic models, respectively (Figure 4B – C). The estimated PSO and PFO kinetic

319 parameters can be found in SI, Table S4. The $v(PO)$- and $v(CAc)$-associated adsorption rate

320 constants ($k_{2(PO),ads}$ and $k_{2,(CAc)ads}$) decreased with increasing PS surface loading on PS-goethite

321 although higher PS loadings had less of an effect. These results suggest glyphosate's access to

322 the active sites on goethite was diminished by the primary layer of PS adsorbed at the goethite

323 surface [12]. For the first time, our kinetic modeling shows the carboxylate-amine groups of

324 glyphosate interact with faster kinetics compared to the phosphonate group, particularly at PS

325 surface loadings ≤ 14 μM (Table S4). The fact that different IR bands of the same molecule (i.e.,

326 glyphosate) evolve at different rates indicates the presence of more than one interfacial species or

327 it might be caused by interaction with different sites on these heterogeneous surfaces [30, 55]. As

328 shown in Figure 4D, the fraction of $v(CAc)$ IR bands retained after desorption increased with

329 increasing PS loading whereas that of $v(PO)$ decreased initially but then increased to a value

330 similar to goethite (≥ 28 μM). This behavior suggests PS-goethite associations may hinder

331   desorption of glyphosate at higher PS loading and is in agreement with retained glyphosate

332   values in batch experiments (Figure 3A). Still, desorption rate constants ($k_{1,(PO)des}$ and $k_{1,(CAc)des}$)

333   show similar kinetic trends, with the carboxylate-amine groups presenting slower desorption

334   rates at low PS loadings (Table S4). Moreover, adsorbed PS was reduced by 8.5 – 23.5 % upon

335   introduction of glyphosate at the stabilized PS-goethite interface (Figure S5) whereas no

336   significant changes to the ATR-FTIR spectra of PS-goethite were observed in control

337   experiments after the introduction of 10 mM KCl background solution (Figure S6). These results

338   suggest glyphosate, and potentially other low molecular weight organics, might have a

339   destabilizing effect on OMAs present in soils [56, 57].

340   The most striking results were found when the $v(CAc)$ bands were deconvoluted across all

341   experiments (Figure S7, Figure 5). The carboxylate-amine band ($v(CAc)$) of glyphosate (1700 –

342   1550 cm^{-1}) originates mainly from asymmetrical stretching vibration modes of COO$^-$ and its

343   coupling with deformation modes of the NH$_2^+$ group [7, 8, 21, 58]. The carboxylate-amine

344   coupling ($v(CAc)$) can therefore be deconvoluted into four tentative vibrational modes, including

345   two COO$^-$ stretching and two NH$_2^+$ deformation vibration modes [8]:

$$v(CAc) = \left(v_{as}\left(COO^-\right)_I + v_{as}\left(COO^-\right)_{II} + \delta\left(NH_2^+\right)_I + \delta\left(NH_2^+\right)_{II} \right) \qquad \text{(Eq. 3)}$$

346   After deconvolution of the $v(CAc)$ band, individual contributions to surface-associated

347   glyphosate, X, at the end of adsorption and desorption phases were calculated using the following

348   equation:

$$X = \left(\frac{A_e(\tilde{v}_i)}{A_e(CAc)} \right) \times 100 \qquad \text{(Eq. 4)}$$

349   where, $A_e(CAc)$ is the integral $v(CAc)$ band and $A_e(\tilde{v}_i)$ is the integral of deconvoluted components

350   of $v_{as}(COO^-)$ (i.e., [$v_{as}(COO^-)_I + v_{as}(COO^-)_{II}$]) or $\delta(NH_2^+)$ (i.e., [$\delta(NH_2^+)_I + \delta(NH_2^+)_{II}$]) bands.

17

351   We found glyphosate's $\delta(NH_2^+)$ band contribution to adsorption ($X(\delta(NH_2^+)_{ads})$ increased as a

352   function of PS surface loading, from 28 % to 45 % (Figure 5A-1). Conversely, glyphosate

353    $v_{as}(COO^-)$ band contribution to adsorption ($X(v(COO^-)_{ads})$ diminished with increasing PS surface

354   loading, from 72 % to 55 %. Although similar trends were observed during the desorption phase

355   (Figure 5A-2), the remaining surface-associated $X(\delta(NH_2^+)$ increased with increasing PS surface

356   loading ([PS] $\geq$ 28 µM) to $\approx$ 60 %. The remaining surface-associated $X(v(COO^-)_{des}$ diminished to

357    $\approx$ 40 % at PS loadings $\geq$ 28 µM. Furthermore, Figure 5B-1 to B-4 and Table S5 indicate surface-

358   associated $\delta(NH_2^+)$ adsorption bands of glyphosate evolved faster than corresponding $v_{as}(COO^-)$

359   bands at higher PS surface loadings (PS $\geq$ 28 µM). This can be explained by the interfacial

360   electrostatic potential, which is expected to increase for a positive functional group with

361   increasing PS surface loading due to the increased number of carboxylate functionalities

362   available in PS chains (PS used in experiments had an estimated $\approx$ 37% carboxylate content; see

363   SM1). Interactions between glyphosate-NH_2^+ and O-containing residues in PS chains are

364   therefore deemed favorable through hydrogen bonding and electrostatic interactions [16, 49, 59,

365   60].

366
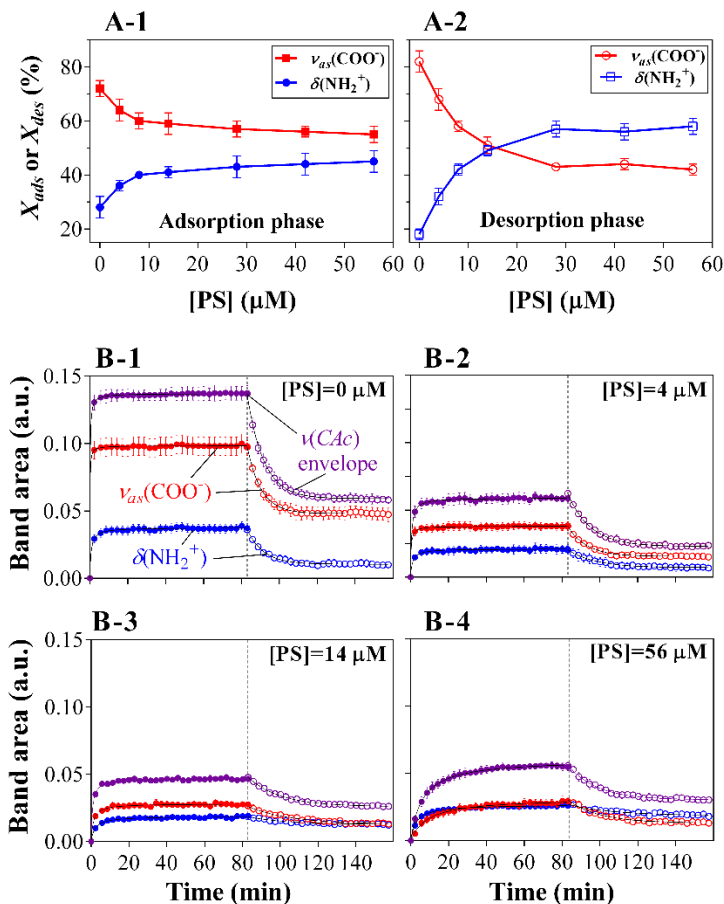
Figure 5. Contribution *(X_{ads} and X_{des})* of deconvoluted *v(CAc)* band components of glyphosate at

(A-1) adsorption ($t_{e,ads}$ = 80.0 min) and (A-2) desorption ($t_{e,des}$ = 157.5 min) equilibrium as a

function of PS loading. (B) shows the evolution of *v(CAc)* glyphosate band components during

adsorption and desorption for (B-1) goethite and (B-2 to B-4) PS-goethite OMAs with increased

PS loading. Black lines in B represent PSO and PFO kinetic fits for adsorption and desorption,

respectively. Dashed vertical lines split glyphosate's adsorption and desorption phases.

373

3.5. Mechanisms of interaction

3.5.1. Phosphonate-meditated binding

19

376   The predominant species of glyphosate at pH 5.0 and $I = 10$ mM is the monoanion [$^-$

377    $OOCCH_2N^+H_2CH_2-HPO_3^-$] (69.78 %), with lesser contributions from its dianion [$^-$

378    $OOCCH_2N^+H_2CH_2-PO_3^{2-}$] (30.09 %) and trianion [$^-OOCCH_2NHCH_2-PO_3^{2-}$] (0.13 %) species

379   ($pK_{a2} = 2.3$, $pK_{a3} = 5.5$ and $pK_{a4} = 11.0$) [19, 61, 62]. Therefore, glyphosate has the capacity to

380   interact with goethite and PS-goethite interfaces through various functionalities to form surface-

381   associated species of different geometries (Figure 4A-1 and A-2, and Table S6) [4, 7-9, 12, 14,

382   20, 21, 63]. The interfacial ATR spectra indicate that Fe-O-P bonds (i.e., *IS* complex) formed at

383   the goethite interface ($1050 - 950$ cm^{-1}). It has been suggested that under slightly acidic

384   conditions (e.g., pH=5) the phosphonate group of glyphosate forms *IS* complexes with goethite,

385   more favorably bidentate (*B*) and monodentate with proton (*M-H*), through ligand-exchange

386   reactions [8, 9, 14]. At pH = 5.0, the electrostatic attraction potential at the goethite surface

387   ($pH_{pzc} = 8.4 \pm 0.2$) increases the energetic favorability to form bidentate complexes through

388   phosphonate groups. Furthermore, our study indicates that an *IS* monodentate complex without

389   proton (*M*) most likely forms due to the contribution of glyphosate's dianion species [8, 14].

390   Besides reducing the number of available surface sites, adsorption of PS diminishes the

391   electrostatic interaction energy between glyphosate's phosphonate group and the goethite surface

392   [64] thus promoting the formation of *IS* monodentate complexes over bidentate. In addition,

393   increase PS loading on PS-goethite OMAs increases the surface negative charge that favors the

394   formation of monodentate complexes [8, 9, 14]. Since the phosphonate anion is a strong acceptor

395   of hydrogen bonds [65], the downshift for unbonded $v(P=O)$ (≈ 8 cm^{-1}) in PS-goethite OMAs

396   (Figure 4A-2, Table S6) is expected to result from intermolecular hydrogen bonds formed

397   between glyphosate's phosphonate group and PS residues in OMAs. Moreover, a new IR feature

398   is observed in ATR-FTIR spectra of PS-goethite OMAs at $1160 - 1164$ cm^{-1}. We tentatively

399   assign this new feature to outer-sphere (*OS*) complexes ($\nu_{as}(PO_2)_{PS\text{-}OS}$; i.e., R-PO$_3^-$(H) $\cdots$ O/N-

400   PS) which split at lower energies due to hydrogen bonding (Figure 4A-2). These results are in

401   agreement with high-resolution P 2p XPS spectra (Figure 6) where increases in binding energy

402   (B.E.) of the P atom 2p envelop upon glyphosate adsorption on goethite (+0.5 eV) and PS-

403   goethite OMAs (+0.5 – +0.1 eV) are observed. Increases in B.E. result from decreases in

404   electron density in the P atom of the phosphonate group that occur upon formation of mixed

405   bidentate-monodentate Fe-O-P bonds [66-68]. Greater shifts in P 2p binding energy are

406   associated with bidentate configuration, as is the case for phosphonate group binding on goethite

407   [69].
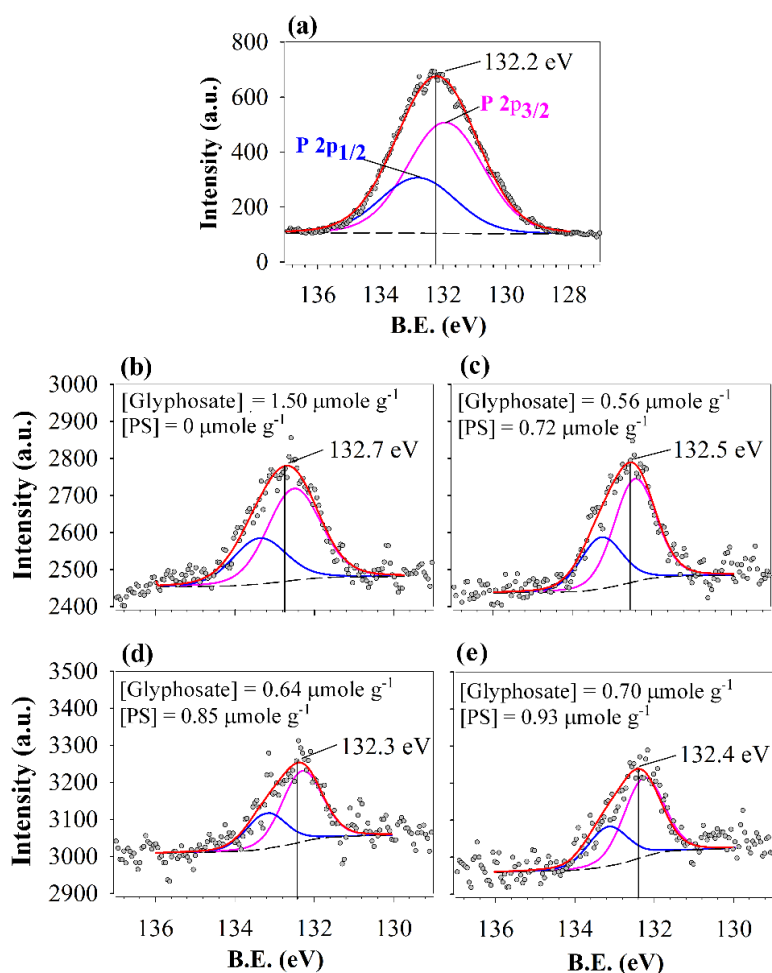
408

409   **Figure 6.** High resolution P 2p XPS spectra for (a) standard glyphosate salt, (b) glyphosate

410   adsorbed on goethite, and (c – e) glyphosate adsorbed on PS-goethite OMAs. The P 2p spectrum

411   of glyphosate presents two component peaks centered at 131.9 ($2p_{3/2}$) and 132.8 ($2p_{1/2}$) eV,

412   which are associated with the spin-orbit splitting of the P 2p level, with a separation of ≈ 0.9 eV

413   [70]. Solid vertical lines indicate the B.E. of the P 2p XPS spectra envelope.

414

3.5.2. Carboxylate and amine-meditated binding

416   Changes in peak position of the carboxylate ($v_{as}(COO^-)$ and $v_s(COO^-)$) and amine ($\delta(NH_2^+)$)

417   vibrational modes of glyphosate are used to decipher carboxylate- and amine-meditated

418   molecular interactions at the goethite and PS-goethite interface [7, 8, 21, 58]. At the goethite

419   interface, both asymmetric and symmetric vibrational modes of the carboxylate group of sorbed

420   glyphosate were subjected to downward shifts (6 –15 cm^{-1}) (Figure 4, A-1, and Table S6). Albeit

421   to a lesser extent, downward shifts in $v(COO^-)$ were also observed at the PS-goethite interface

422   (Figure 4, A-2, and Table S6). A reduction in $v(COO^-)$ vibrational energy suggest glyphosate's

423   carboxylate group primarily contributes to the formation of *OS* complexes via intermolecular

424   hydrogen bonding that occurs among glyphosate molecules at the goethite surface. These

425   observations are in agreement with previous studies where the adsorption modes of carboxylate-

426   containing organic anions and zwitterions (including glyphosate) on goethite have been

427   investigated [8, 9, 12, 21, 58, 71-73].

428   As in previous studies [9, 14], we found no evidence for the participation of the NH_2^+ group of

429   glyphosate in surface complexation at the goethite interface (Figure 4, A-1, and Table S6).

430   Interfacial $\delta(NH_2^+)$ vibrational modes of glyphosate however shifted to higher energies (by 7-27

431   cm^{-1}) at the PS-goethite interface (Figure 4, A-2, and Table S6). These bands also gained

432   intensity relative to interfacial v_{as}(COO$^-$) bands as a function of PS surface loading (Figure 5 and

433   Table S5). The abovementioned observations imply glyphosate forms amine-associated

434   hydrogen bonds with PS-goethite OMAs since hydrogen bonds stabilize charged resonance

435   structures [74] and the strength of hydrogen bonds is related to the integrated absorbance of

436   amine bands [60]. Therefore, the corresponding upshifts with increasing PS surface loading

437   denote the involvement of the amine group through stronger hydrogen bonds with carbonyl-

438   containing functional groups of the polysaccharide. Although glyphosate NH$_2^+$ group is expected

439   to encounter a repulsive force from the mostly positive-charged goethite surface that establish a

440   barrier for amine-meditated hydrogen bonding, the presence of PS associations may facilitate

441   these interactions due to the development of a negative charge at the surface of PS-goethite

442   OMAs (Figure 3B).

443

444   **4. Conclusions**

445   Studies of glyphosate retention dynamics at organo-mineral interfaces, as presented in this

446   work, are environmentally relevant since surface soils contain minerals that are mostly, if not

447   completely, coated with organic molecules. While the fate of glyphosate in soils is strongly

448   influenced by organic-organic interactions (e.g., glyphosate-polysaccharide) that occur with

449   organo-mineral associations (e.g., polysaccharide-goethite), research in this area is still limited

450   and the results inconclusive. Our work contributes to the narrowing of this considerable

451   knowledge gap [8, 12, 16].

452   Using model organo-mineral associations (i.e., polysaccharide-goethite OMAs), our

453   experiments indicate the amount of mineral-adsorbed organic matter modulates the extent,

454   kinetics, and mechanisms of interaction of glyphosate under conditions relevant to agricultural

455   soils of humid regions. The extent of glyphosate retention at polysaccharide-goethite interfaces

456   was reduced compared to that at the goethite interface. At the same time, increased

457   polysaccharide surface loading resulted in slower glyphosate adsorption and desorption kinetics

458   compared to corresponding processes at the goethite interface. Mechanistically, increases in PS

459   surface loading resulted in the successive disappearance of glyphosate inner-sphere bidentate

460   configurations on goethite while promoting the formation of inner-sphere monodentate

461   configurations. Furthermore, the adsorbed polysaccharide promoted the formation of outer-

462   sphere surface species through intermolecular hydrogen bonds between the functional groups of

463   glyphosate and functional groups at goethite and polysaccharide-goethite interfaces. Based on

464   the results of this investigation, we suggest studies with bare mineral surfaces [9, 32, 75-77] are

465   likely to underestimate glyphosate mobility and transport in soils since organo-mineral

466   associations can reduce both the adsorption capacity and kinetics, in addition to promoting the

467   formation of presumably weaker mechanisms of interaction.

468   The results of these studies highlight the impact organo-mineral associations might have on

469   glyphosate's mobility and retention at heterogeneous interfaces present in soils. But since the

470   proportion of organo-mineral to mineral interfaces is higher in surface soils, our work provides

471   insights as to the extent, kinetics and mechanisms that might be involved during glyphosate

472   downward transport. Ultimately, this knowledge and further molecular-scale studies with a

473   variety of organo-mineral interfaces could lead to better predictions of glyphosate occurrence in

474   natural systems and risk assessments.

475

476   **Acknowledgments and Funding**

489

490 **Author contributions statement**

491 B.A. conceptualized and led the laboratory work, produced, and interpreted data and led

492 manuscript writing. C.E.M. conceptualized research and secured the funding, supervised the

493 project, and provided critical revision of the manuscript.

494

495 **Declaration of competing interest**

496 The authors declare that they have no known competing financial interests or personal

497 relationships that could have appeared to influence the work reported in this paper.

498

499 **Appendix A. Supplementary information**

500

Data availability

502   Data will be made available on request.

503

References

505   [1] P. Nadin, The use of plant protection products in the European union data 1992–2003,
506   European Commission: Luxembourg, France (2007).
507   [2] H. Li, A.F. Wallace, M. Sun, P. Reardon, D.P. Jaisi, Degradation of glyphosate by Mn-oxide
508   may bypass sarcosine and form glycine directly after C–N bond cleavage, Environmental science
509   & technology 52(3) (2018) 1109-1117.
510   [3] C. Huhn, More and enhanced glyphosate analysis is needed, Analytical and bioanalytical
511   chemistry 410(13) (2018) 3041-3045.
512   [4] T. Undabeytia, E. Morillo, C. Maqueda, FTIR Study of Glyphosate−Copper Complexes,
513   Journal of Agricultural and Food Chemistry 50(7) (2002) 1918-1921.
514   [5] V. Subramaniam, P.E. Hoggard, Metal complexes of glyphosate, Journal of agricultural and
515   food chemistry 36(6) (1988) 1326-1329.
516   [6] J. Sheals, P. Persson, B. Hedman, IR and EXAFS Spectroscopic Studies of Glyphosate
517   Protonation and Copper(II) Complexes of Glyphosate in Aqueous Solution, Inorganic Chemistry
518   40(17) (2001) 4302-4309.
519   [7] B.C. Barja, M. dos Santos Afonso, An ATR−FTIR Study of Glyphosate and Its Fe(III)
520   Complex in Aqueous Solution, Environmental Science & Technology 32(21) (1998) 3331-3335.
521   [8] W. Yan, C. Jing, Molecular Insights into Glyphosate Adsorption to Goethite Gained from
522   ATR-FTIR, Two-Dimensional Correlation Spectroscopy, and DFT Study, Environmental
523   science & technology 52(4) (2018) 1946-1953.
524   [9] J. Sheals, S. Sjöberg, P. Persson, Adsorption of glyphosate on goethite: molecular
525   characterization of surface complexes, Environmental science & technology 36(14) (2002) 3090-
526   3095.
527   [10] E.J. Elzinga, D.L. Sparks, Phosphate adsorption onto hematite: An in situ ATR-FTIR
528   investigation of the effects of pH and loading level on the mode of phosphate surface
529   complexation, Journal of Colloid and Interface Science 308(1) (2007) 53-70.
530   [11] C.N. Albers, G.T. Banta, P.E. Hansen, O.S. Jacobsen, The influence of organic matter on
531   sorption and fate of glyphosate in soil–Comparing different soils and humic substances,
532   Environmental pollution 157(10) (2009) 2865-2870.
533   [12] J.M. Arroyave, C.C. Waiman, G.P. Zanini, M.J. Avena, Effect of humic acid on the
534   adsorption/desorption behavior of glyphosate on goethite. Isotherms and kinetics, Chemosphere
535   145 (2016) 34-41.
536   [13] K.A. Barrett, M.B. McBride, Oxidative Degradation of Glyphosate and
537   Aminomethylphosphonate by Manganese Oxide, Environmental Science & Technology 39(23)
538   (2005) 9223-9228.

[14] B.C. Barja, M. dos Santos Afonso, Aminomethylphosphonic Acid and Glyphosate Adsorption onto Goethite: A Comparative Study, Environmental Science & Technology 39(2) (2005) 585-592.

[15] R.L. Glass, Adsorption of glyphosate by soils and clay minerals, Journal of Agricultural and Food Chemistry 35(4) (1987) 497-500.

[16] F. Guo, M. Zhou, J. Xu, J.B. Fein, Q. Yu, Y. Wang, Q. Huang, X. Rong, Glyphosate adsorption onto kaolinite and kaolinite-humic acid composites: Experimental and molecular dynamics studies, Chemosphere 263 (2021) 127979.

[17] R. Sutton, G. Sposito, Molecular structure in soil humic substances: the new view, Environmental science & technology 39(23) (2005) 9009-9015.

[18] M. McBride, K.-H. Kung, Complexation of Glyphosate and Related Ligands with Iron (III), Soil Science Society of America Journal 53(6) (1989) 1668-1673.

[19] L. Tribe, K.D. Kwon, C.C. Trout, J.D. Kubicki, Molecular orbital theory study on surface complex structures of glyphosate on goethite: calculation of vibrational frequencies, Environmental science & technology 40(12) (2006) 3836-3841.

[20] C.V. Waiman, M.J. Avena, A.E. Regazzoni, G.P. Zanini, A real time in situ ATR-FTIR spectroscopic study of glyphosate desorption from goethite as induced by phosphate adsorption: Effect of surface coverage, Journal of Colloid and Interface Science 394 (2013) 485-489.

[21] Y. Yang, S. Wang, Y. Xu, B. Zheng, J. Liu, Molecular-Scale Study of Aspartate Adsorption on Goethite and Competition with Phosphate, Environmental Science & Technology 50(6) (2016) 2938-2945.

[22] I. Kögel-Knabner, The macromolecular organic composition of plant and microbial residues as inputs to soil organic matter, Soil Biology and Biochemistry 34(2) (2002) 139-162.

[23] N. Manucharova, The microbial destruction of chitin, pectin, and cellulose in soils, Eurasian Soil Science 42(13) (2009) 1526-1532.

[24] D. Mohnen, Pectin structure and biosynthesis, Current Opinion in Plant Biology 11(3) (2008) 266-277.

[25] A.K. Chatjigakis, C. Pappas, N.Proxenia, O.Kalantzi, P.Rodis, M. Polissiou, FT-IR spectroscopic determination of the degree of esterification of cell wall pectins from stored peaches and correlation to textural changes, Carbohydrate Polymers 37(4) (1998) 395-408.

[26] E. De Gerónimo, V.C. Aparicio, Changes in soil pH and addition of inorganic phosphate affect glyphosate adsorption in agricultural soil, European Journal of Soil Science 73(1) (2022) e13188.

[27] B. Zhao, J. Zhang, J. Gong, H. Zhang, C. Zhang, Glyphosate mobility in soils by phosphate application: Laboratory column experiments, Geoderma 149(3) (2009) 290-297.

[28] R.C. Pereira, P.R. Anizelli, E. Di Mauro, D.F. Valezi, A.C.S. da Costa, C.T.B.V. Zaia, D.A.M. Zaia, The effect of pH and ionic strength on the adsorption of glyphosate onto ferrihydrite, Geochemical Transactions 20(1) (2019) 3.

[29] M.P. Schmidt, C.E. Martínez, Supramolecular association impacts biomolecule adsorption onto goethite, Environmental science & technology 52(7) (2018) 4079-4089.

[30] M.P. Schmidt, S.D. Siciliano, D. Peak, Spectroscopic Quantification of Inner- and Outer-Sphere Oxyanion Complexation Kinetics: Ionic Strength and Background Cation Effect on Sulfate Adsorption to Hematite, ACS Earth and Space Chemistry 4(10) (2020) 1765-1776.

[31] M.P. Schmidt, C.E. Martínez, Ironing Out Genes in the Environment: An Experimental Study of the DNA–Goethite Interface, Langmuir 33(34) (2017) 8525-8532.

584 [32] C.V. Waiman, J.M. Arroyave, H. Chen, W. Tan, M.J. Avena, G.P. Zanini, The simultaneous
585 presence of glyphosate and phosphate at the goethite surface as seen by XPS, ATR-FTIR and
586 competitive adsorption isotherms, Colloids and Surfaces A: Physicochemical and Engineering
587 Aspects 498 (2016) 121-127.
588 [33] P. Mazzei, A. Piccolo, Quantitative evaluation of noncovalent interactions between
589 glyphosate and dissolved humic substances by NMR spectroscopy, Environmental science &
590 technology 46(11) (2012) 5939-5946.
591 [34] C.A. Hettiarachchi, L.D. Melton, M.A. Williams, D.J. McGillivray, J.A. Gerrard, S.M.
592 Loveday, M orphology of complexes formed between β-lactoglobulin nanofibrils and pectins is
593 influenced by the pH and structural characteristics of the pectins, Biopolymers 105(11) (2016)
594 819-831.
595 [35] B.M. Yapo, Rhamnogalacturonan-I: a structurally puzzling and functionally versatile
596 polysaccharide from plant cell walls and mucilages, Polymer Reviews 51(4) (2011) 391-413.
597 [36] D.A. Méndez, M.J. Fabra, L. Gómez-Mascaraque, A. López-Rubio, A. Martinez-Abad,
598 Modelling the Extraction of Pectin towards the Valorisation of Watermelon Rind Waste, Foods
599 10(4) (2021) 738.
600 [37] P.L. Rockwell, M.A. Kiechel, J.S. Atchison, L.J. Toth, C.L. Schauer, Various-sourced
601 pectin and polyethylene oxide electrospun fibers, Carbohydrate Polymers 107 (2014) 110-118.
602 [38] U. Schwertmann, R.M. Cornell, Iron oxides in the laboratory: preparation and
603 characterization, John Wiley & Sons2008.
604 [39] A. Viegas, J. Manso, F.L. Nobrega, E.J. Cabrita, Saturation-Transfer Difference (STD)
605 NMR: A Simple and Fast Method for Ligand Screening and Characterization of Protein Binding,
606 Journal of Chemical Education 88(7) (2011) 990-994.
607 [40] T.C. Catrinck, A. Dias, M.C.S. Aguiar, F.O. Silvério, P.H. Fidêncio, G.P. Pinho, A simple
608 and efficient method for derivatization of glyphosate and AMPA using 9-fluorenylmethyl
609 chloroformate and spectrophotometric analysis, Journal of the Brazilian Chemical Society 25
610 (2014) 1194-1199.
611 [41] D.E. Felton, M. Ederer, T. Steffens, P.L. Hartzell, K.V. Waynant, UV–Vis
612 Spectrophotometric Analysis and Quantification of Glyphosate for an Interdisciplinary
613 Undergraduate Laboratory, Journal of Chemical Education 95(1) (2018) 136-140.
614 [42] Y.-S. Ho, Review of second-order models for adsorption systems, Journal of hazardous
615 materials 136(3) (2006) 681-689.
616 [43] W. Plazinski, W. Rudzinski, A. Plazinska, Theoretical models of sorption kinetics including
617 a surface reaction mechanism: A review, Advances in Colloid and Interface Science 152(1)
618 (2009) 2-13.
619 [44] S. Lagergren, Zur theorie der sogenannten adsorption geloster stoffe, (1898).
620 [45] B. Cartigny, N. Azaroual, M. Imbenotte, D. Mathieu, G. Vermeersch, J.P. Goullé, M.
621 Lhermitte, Determination of glyphosate in biological fluids by 1H and 31P NMR spectroscopy,
622 Forensic Science International 143(2) (2004) 141-145.
623 [46] K. Ariga, T. Kunitake, Supramolecular chemistry-fundamentals and applications: advanced
624 textbook, Springer Science & Business Media2006.
625 [47] A. Synytsya, J. Čopíková, P. Matějka, V. Machovič, Fourier transform Raman and infrared
626 spectroscopy of pectins, Carbohydrate Polymers 54(1) (2003) 97-106.
627 [48] I. Šimkovic, A. Synytsya, I. Uhliariková, J. Čopíková, Amidated pectin derivatives with n-
628 propyl-, 3-aminopropyl-, 3-propanol- or 7-aminoheptyl-substituents, Carbohydrate Polymers
629 76(4) (2009) 602-606.

[49] A. Sinitsya, J. Čopíková, V. Prutyanov, S. Skoblya, V. Machovič, Amidation of highly methoxylated citrus pectin with primary amines, Carbohydrate Polymers 42(4) (2000) 359-368.

[50] F. Meneguzzo, C. Brunetti, A. Fidalgo, R. Ciriminna, R. Delisi, L. Albanese, F. Zabini, A. Gori, L.B. dos Santos Nascimento, A. De Carlo, F. Ferrini, L.M. Ilharco, M. Pagliaro, Real-Scale Integral Valorization of Waste Orange Peel via Hydrodynamic Cavitation, Processes 7(9) (2019) 581.

[51] A. Fidalgo, R. Ciriminna, D. Carnaroglio, A. Tamburino, G. Cravotto, G. Grillo, L.M. Ilharco, M. Pagliaro, Eco-Friendly Extraction of Pectin and Essential Oils from Orange and Lemon Peels, ACS Sustainable Chemistry & Engineering 4(4) (2016) 2243-2251.

[52] A. Assifaoui, C. Loupiac, O. Chambin, P. Cayot, Structure of calcium and zinc pectinate films investigated by FTIR spectroscopy, Carbohydrate Research 345(7) (2010) 929-933.

[53] M.H.G. Canteri, C.M.G.C. Renard, C. Le Bourvellec, S. Bureau, ATR-FTIR spectroscopy to determine cell wall composition: Application on a large diversity of fruits and vegetables, Carbohydrate Polymers 212 (2019) 186-196.

[54] S. Guzman-Puyol, J.J. Benítez, E. Domínguez, I.S. Bayer, R. Cingolani, A. Athanassiou, A. Heredia, J.A. Heredia-Guerrero, Pectin-Lipid Self-Assembly: Influence on the Formation of Polyhydroxy Fatty Acids Nanoparticles, PLOS ONE 10(4) (2015) e0124639.

[55] A.G. Young, A.J. McQuillan, Adsorption/Desorption Kinetics from ATR-IR Spectroscopy. Aqueous Oxalic Acid on Anatase TiO2, Langmuir 25(6) (2009) 3538-3548.

[56] M. Keiluweit, J.J. Bougoure, P.S. Nico, J. Pett-Ridge, P.K. Weber, M. Kleber, Mineral protection of soil carbon counteracted by root exudates, Nature Climate Change 5(6) (2015) 588-595.

[57] Y. Yuan, Z. Zhang, L. Chen, Z. Yang, J. Liu, Facilitated destabilization of physicochemically protected soil organic matter by root-derived low-molecular-weight organic acids, Journal of Soils and Sediments 22(6) (2022) 1677-1686.

[58] K. Norén, J.S. Loring, P. Persson, Adsorption of alpha amino acids at the water/goethite interface, Journal of Colloid and Interface Science 319(2) (2008) 416-428.

[59] Z. Gu, R. Zambrano, A. McDermott, Hydrogen Bonding of Carboxyl Groups in Solid-State Amino Acids and Peptides: Comparison of Carbon Chemical Shielding, Infrared Frequencies, and Structures, Journal of the American Chemical Society 116(14) (1994) 6368-6372.

[60] F.C. Wang, M. Feve, T.M. Lam, J.-P. Pascault, FTIR analysis of hydrogen bonding in amorphous linear aromatic polyurethanes. I. Influence of temperature, Journal of Polymer Science Part B: Polymer Physics 32(8) (1994) 1305-1313.

[61] W. Li, Y.-J. Wang, M. Zhu, T.-T. Fan, D.-M. Zhou, B.L. Phillips, D.L. Sparks, Inhibition Mechanisms of Zn Precipitation on Aluminum Oxide by Glyphosate: A 31P NMR and Zn EXAFS Study, Environmental Science & Technology 47(9) (2013) 4211-4219.

[62] Z. Chen, W. He, M. Beer, M. Megharaj, R. Naidu, Speciation of glyphosate, phosphate and aminomethylphosphonic acid in soil extracts by ion chromatography with inductively coupled plasma mass spectrometry with an octopole reaction system, Talanta 78(3) (2009) 852-856.

[63] M.C. Zenobi, C.V. Luengo, M.J. Avena, E.H. Rueda, An ATR-FTIR study of different phosphonic acids in aqueous solution, Spectrochimica Acta Part A: Molecular and Biomolecular Spectroscopy 70(2) (2008) 270-276.

[64] H.-X. Zhou, X. Pang, Electrostatic Interactions in Protein Structure, Folding, Binding, and Condensation, Chemical Reviews 118(4) (2018) 1691-1741.

[65] W. Pohle, M. Bohl, H. Böhlig, Interpretation of the influence of hydrogen bonding on the stretching vibrations of the PO_2^- moiety, Journal of Molecular Structure 242 (1991) 333-342.

676 [66] L. Zhang, Y. Liu, Y. Wang, X. Li, Y. Wang, Investigation of phosphate removal
677 mechanisms by a lanthanum hydroxide adsorbent using p-XRD, FTIR and XPS, Applied Surface
678 Science 557 (2021) 149838.
679 [67] Y. Guo, J. Yu, X. Li, L. Guo, C. Xiao, R. Chi, H. Hou, G. Feng, Selective recovery of
680 glyphosine from glyphosate mother liquor using a modified biosorbent: Competitive substitution
681 adsorption, Environmental Research 215 (2022) 114394.
682 [68] M. Mallet, K. Barthélémy, C. Ruby, A. Renard, S. Naille, Investigation of phosphate
683 adsorption onto ferrihydrite by X-ray Photoelectron Spectroscopy, Journal of Colloid and
684 Interface Science 407 (2013) 95-101.
685 [69] M. Wagstaffe, A.G. Thomas, M.J. Jackman, M. Torres-Molina, K.L. Syres, K. Handrup, An
686 experimental investigation of the adsorption of a phosphonic acid on the anatase TiO2 (101)
687 surface, The Journal of Physical Chemistry C 120(3) (2016) 1693-1700.
688 [70] B.D. Ratner, D.G. Castner, Electron spectroscopy for chemical analysis, Surface analysis:
689 the principal techniques 2 (2009) 374-381.
690 [71] B. Barja, M. dos Santos Afonso, Aminomethylphosphonic acid and glyphosate adsorption
691 onto goethite: a comparative study, Environmental science & technology 39(2) (2005) 585-592.
692 [72] J. Liang, J.H. Horton, Interactions of Benzoic Acid and Phosphates with Iron Oxide
693 Colloids Using Chemical Force Titration, Langmuir 21(23) (2005) 10608-10614.
694 [73] K. Norén, P. Persson, Adsorption of monocarboxylates at the water/goethite interface: The
695 importance of hydrogen bonding, Geochimica et Cosmochimica Acta 71(23) (2007) 5717-5730.
696 [74] N.S. Myshakina, Z. Ahmed, S.A. Asher, Dependence of Amide Vibrations on Hydrogen
697 Bonding, The Journal of Physical Chemistry B 112(38) (2008) 11873-11877.
698 [75] G.A. Khoury, T.C. Gehris, L. Tribe, R.M.T. Sánchez, M. dos Santos Afonso, Glyphosate
699 adsorption on montmorillonite: An experimental and theoretical study of surface complexes,
700 Applied Clay Science 50(2) (2010) 167-175.
701 [76] A.A. Ahmed, P. Leinweber, O. Kühn, Unravelling the nature of glyphosate binding to
702 goethite surfaces by ab initio molecular dynamics simulations, Physical Chemistry Chemical
703 Physics 20(3) (2018) 1531-1539.
704 [77] E. Morillo, T. Undabeytia, C. Maqueda, Adsorption of glyphosate on the clay mineral
705 montmorillonite: effect of Cu (II) in solution and adsorbed on the mineral, Environmental
706 science & technology 31(12) (1997) 3588-3592.

707